Charge transport and intrinsic fluorescence in amyloid-like fibrils

Loretta Laureana del Mercato*†, Pier Paolo Pompa*†, Giuseppe Maruccio*, Antonio Della Torre*, Stefania Sabella*, Antonio Mario Tamburro‡, Roberto Cingolani*, and Ross Rinaldi*

*National Nanotechnology Laboratory, Istituto Nazionale per la Fisica della Materia-Consiglio Nazionale della Ricerche, and Italian Institute of Technology (IIT) Research Unit, Scuola Superiore ISUFI, University of Salento, Via per Arnesano, 73100 Lecce, Italy; and ‡Department of Chemistry, University of Basilicata, Via N. Sauro, 85100 Potenza, Italy

Edited by David Baker, University of Washington, Seattle, WA, and approved September 20, 2007 (received for review March 27, 2007)

The self-assembly of polypeptides into stable, conductive, and intrinsically fluorescent biomolecular nanowires is reported. We have studied the morphology and electrical conduction of fibrils made of an elastin-related polypeptide, poly(ValGlyGlyLeuGly). These amyloid-like nanofibrils, with a diameter ranging from 20 to 250 nm, result from self-assembly in aqueous solution at neutral pH. Their morphological properties and conductivity have been investigated by atomic force microscopy, scanning tunneling microscopy, and two-terminal transport experiments at the micro- and nanoscales. We demonstrate that the nanofibrils can sustain significant electrical conduction in the solid state at ambient conditions and have remarkable stability. We also show intrinsic blue-green fluorescence of the nanofibrils by confocal microscopy analyses. These results indicate that direct (label-free) excitation can be used to investigate the aggregation state or the polymorphism of amyloid-like fibrils (and possibly of other proteinaceous material) and open up interesting perspectives for the use of peptide-based nanowire structures, with tunable physical and chemical properties, for a wide range of nanobiotechnological and bioelectronic applications.

peptide nanostructures | self-assembling | atomic force microscopy | scanning tunneling microscopy | confocal microscopy

Molecular self-assembly is ubiquitous in biological systems and underlies the formation of a wide variety of complex biological structures (1). One important example of self-assembly is the amyloid fibril (2, 3). *In vivo*, amyloids are often associated with disease (4, 5). Amyloid fibrils can be formed by both normal and variant proteins of different origins and with no primary sequence homology (6, 7). They are highly ordered molecular assemblies with similar biophysical and ultrastructural characteristics, including a typical x-ray diffraction pattern and a predominant β-sheet conformation (5, 8–13). The similarity among the different amyloid deposits and their ubiquity suggests that such structures might represent a generic form of the noncovalent packing of polypeptide chains (6, 7, 14). It may be possible that the aggregation into such well defined, nano-ordered assemblies represents a state of an efficient minimal energy arrangement of polypeptide chains (15–17). Recent results have shown that fibrillar structures similar to amyloid fibrils are formed by sequences like poly(XGlyGlyYGly) (X, Y = Val, Leu, or Ala), which are highly repeated in the hydrophobic domains of elastin (18, 19).

Apart from their pathological relevance, amyloid fibrils are one of several self-assembling peptide systems that are attracting increasing interest for applications ranging from molecular electronics (20, 21) to tissue engineering and material science (22–27). Metallic nanowires have been produced by different strategies on templates made from protein nanotubes and nanofibrils (20, 21), and the possibility to control both the vertical and horizontal arrangements of the peptide nanotubes has been demonstrated recently (28). However, electrical conduction in unmetallized fibrils has not been reported. In this paper, we investigated charge transport and intrinsic fluorescence of amyloid-like fibrils made from the synthetic polypentapeptide, poly-(ValGlyGlyLeuGly).

Results and Discussion

Poly(ValGlyGlyLeuGly) amyloid-like fibrils [see supporting information (SI) *Materials and Methods* and SI Fig. 8] were prepared by resuspension in 0.1 mg/ml ultrapure water and examined by atomic force microscopy (AFM) at ambient conditions after deposition onto a SiO_2 substrate and solvent evaporation. We observed protein structures with different sizes, revealing a high degree of conformational heterogeneity of the fibrils upon self-assembling in the water medium (Fig. 1*a*). The diameter of the fibrils was found to be in the 20- to 250-nm range. The presence of some monomers or small aggregates also is visible in the background of the image (Fig. 1*a*). These protein aggregates are thought to fuse into fibrillar structures, although the detailed mechanism underlying the fibrillogenesis process is not yet completely understood (3). AFM measurements showed that poly(ValGlyGlyLeuGly) self-assembles to give fibrils with a characteristic domain texture. Each fibril consists of several protofilaments arranged in a roughly twisted pattern, indicating that they were formed through the lateral alignment of many polypeptide molecules (Fig. 1*b*). A high-resolution AFM image of a single fibril also is reported in Fig. 1*c*. In this case, the biomolecular nanowire is 120 nm in diameter and ≈22 nm in height (see the line profile in Fig. 1*d*). The length of the fibrils varied from hundreds of nanometers to several microns. Tamburro and colleagues (29) recently reported that the filament length of the analogue poly(ValGlyGlyValGly) peptide can reach 70 μm, suggesting a possible mechanism of longitudinal alignment of the peptides besides a lateral one. Repeated AFM imaging performed over the same sample at different times (up to several months after sample preparation) revealed no significant morphological changes, indicating a remarkable stability of the fibrils at ambient conditions, which is in qualitative agreement with our previous data on solid-state protein films (30, 31). AFM analyses also showed that the poly(ValGlyGlyLeuGly) fibrils are stable to heat treatment (80°C with atmospheric pressure for 1 h; 121°C with 1.2 atmospheric pressure for 50 min),

Author contributions: L.L.d.M. and P.P.P. contributed equally to this work; L.L.d.M., P.P.P., G.M., and R.R. designed research; L.L.d.M., P.P.P., G.M., and A.D.T. performed research; A.M.T. contributed new reagents/analytic tools; L.L.d.M., P.P.P., G.M., A.M.T., S.S., R.C., and R.R. analyzed data; and L.L.d.M. and P.P.P. wrote the paper.

The authors declare no conflict of interest.

This article is a PNAS Direct Submission.

Abbreviations: AFM, atomic force microscopy; RH, relative humidity; STM, scanning tunneling microscopy.

†To whom correspondence may be addressed. E-mail: loretta.delmercato@unile.it or piero.pompa@unile.it.

This article contains supporting information online at www.pnas.org/cgi/content/full/0702843104/DC1.

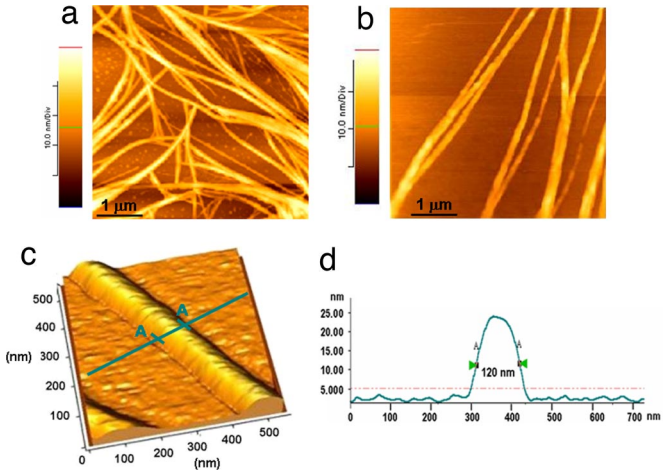

Fig. 1. AFM characterization of poly(ValGlyGlyLeuGly) amyloid-like fibrils. (*a* and *b*) Two representative AFM images of the fibrillar structures onto SiO_2 substrates. (*c*) High-resolution 3D image of a single-peptide nanowire. (*d*) Line profile of the fibril reported in *c*. All AFM experiments were performed at ambient conditions in tapping mode.

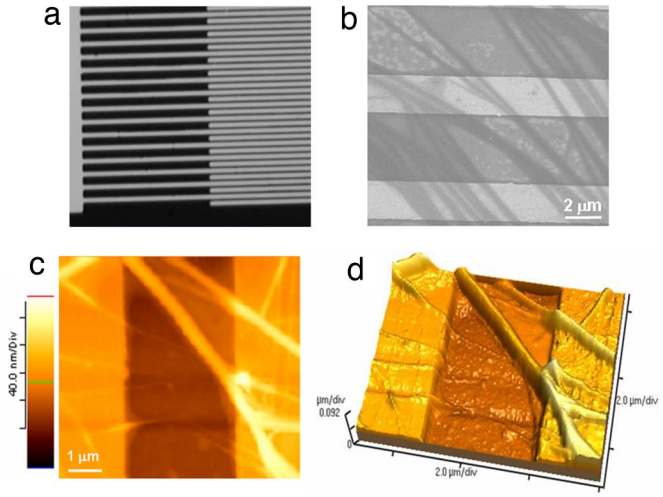

Fig. 3. Charge transport experiments on the nanofibrils. (*a*) SEM image of the interdigitated electrodes used for transport experiments. (*b*) Representative SEM micrograph of the electrodes after fibrils deposition. (*c* and *d*) Two-dimensional (*c*) and 3D (*d*) AFM images of the poly(ValGlyGlyLeuGly) fibrils across the gold electrodes.

as well as to the organic solvents typically used in lithography processes, such as acetone and isopropanol (data not shown).

Protein fibrils also were investigated by scanning tunneling microscopy (STM) experiments. Unmodified fibrils were deposited onto gold substrate to explore their conductive properties and to gain deeper insight into their structure (thanks to the higher imaging resolution of the STM). For these experiments, the 0.1 mg/ml poly(ValGlyGlyLeuGly) fibril suspensions in ultrapure water were deposited onto gold substrates by the same procedure used with silicon dioxide samples. Mature fibrils consisting of several filaments laterally aligned, which interact side by side, were detected (Fig. 2*a*). Each fibril was found to be composed of many polypeptide molecules (Fig. 2*b*), which is in line with previous reports suggesting that amyloid-like fibrils are likely to originate from extensive self-interactions of elemental cross β-structures (19). We also were able to observe fine structural features of the fibrils, such as the characteristic helical twist. Both right-handed (Fig. 2*b*) and left-handed helical orientations were found, which is consistent with a recent study (32).

It is worth noting that the above STM imaging experiments were performed without any metal coating of the proteins,

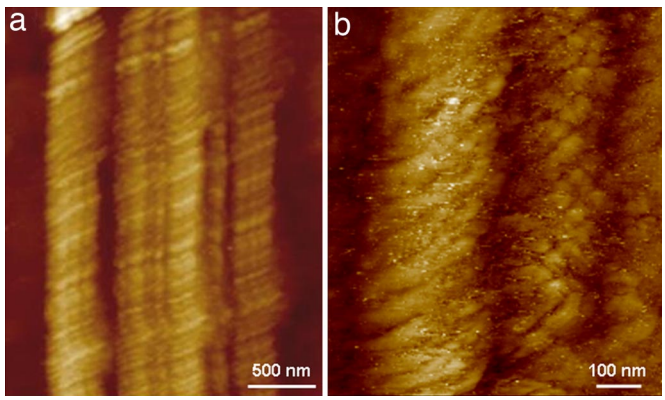

Fig. 2. Two typical high-resolution STM images of poly(ValGlyGlyLeuGly) fibrils deposited onto gold substrates. Experiments were performed in air at room temperature in constant current mode (50–150 pA tunneling current, 0.1 V bias voltage, 1 Hz scan rate).

indicating the ability of unmodified fibrils to sustain electrical conduction. This experimental evidence implies the concept of charge transport processes in these polypeptides molecules. Actually, we recently observed similar findings in disorder multilayers of nonredox proteins (31). Because this class of biomolecular nanowires also was found to be amenable to direct STM imaging, protein conductivity may be considered, in principle, as a rather general phenomenon regardless of the redox functionality of the biomolecule. Remarkably, Wang *et al.* (33) also were able to perform STM experiments on Aβ42 amyloid fibrils without the need for metal coating. Nevertheless, the authors focused their attention on the aggregation processes of the protein structure and did not discuss the physical mechanisms responsible for the fibril conductivity.

In line with our AFM data, STM images were essentially unchanged after several months at ambient conditions, indicating that both the structure and conductivity of the fibrils are marginally affected by aging.

The conductive properties of the fibrils were further investigated by two-terminal transport experiments at ambient conditions. The devices for these measurements consisted of interdigitated electrodes with gaps ranging from 2 to 10 μm (a representative SEM image of a device with a 2-μm interelectrode separation is reported in Fig. 3*a*). The fibrils were deposited onto the electrodes by cast deposition of a 10-μl drop of the 0.1 mg/ml fibrils suspension in ultrapure water. After solvent evaporation, numerous fibrils were seen to span the interelectrode gaps as probed by SEM (Fig. 3*b*) and AFM (Fig. 3 *c* and *d*) analyses. Electrical conductivity was readily detected in these samples. High-current values were recorded, typically in the range of several nA (Fig. 4) depending on the number of fibrils bridging the electrodes and the environmental conditions (the quality of the protein–electrode contacts also plays an important role). Control experiments carried out on empty devices (i.e., without proteins) revealed low-current signals (always <1 pA) (Fig. 4 *Inset*).

A possible qualitative model for the transport mechanism suggests that charges can travel through the self-assembled polypeptides because of the presence of efficient charge-transfer pathways in the fibrillar structures. In particular, a strong role of water molecules in the transport mechanism may be envisaged. It is likely that protein hydration shells are largely retained in the

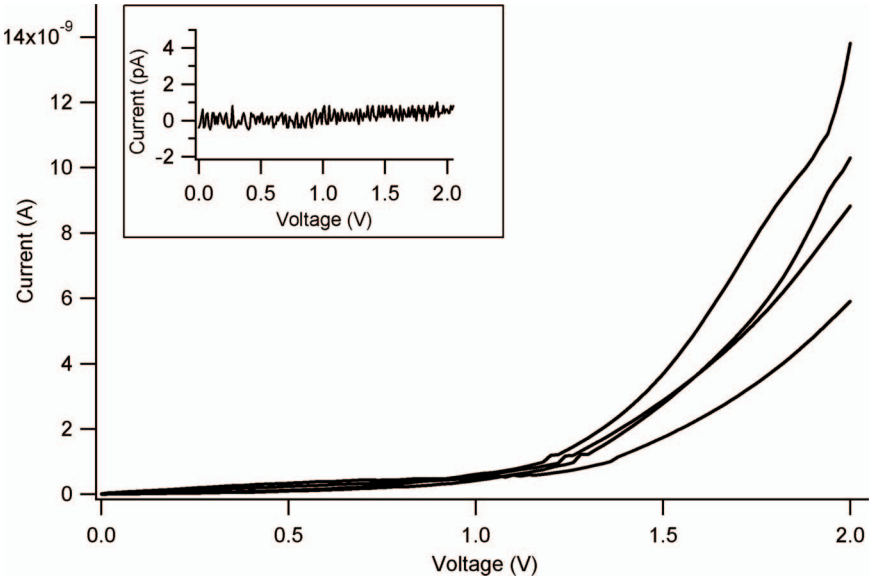

Fig. 4. Typical current–voltage (*I–V*) characteristics of the nanofibrils. (*Inset*) Control experiments carried out on empty devices (i.e., without fibrils), revealing low-current signals (always <1 pA).

solid state and significantly support the intra- and intermolecular charge-transport pathways along the peptides nanowires. Therefore, the formation of continuous molecular chains in the solid-state fibrils may allow for long-range charge transfer between electrodes.

Fibrils samples were characterized in different conditions of humidity [in the 30–70% relative humidity (RH) range]. A strong dependence of the charge-transport behavior on this parameter was observed, with high RH values favoring protein conductivity (the current intensities recorded at ≈70% RH were typically one to two orders of magnitude higher than those detected at ≈30%). Moreover, essentially no conductivity was observed in a vacuum, whereas conductivity was promptly recovered when the samples were brought back to ambient conditions. These results are in qualitative agreement with previous studies on the charge transport in proteins multilayer, where a significant influence of the humidity on the conductance was observed (31). Interestingly, preliminary AFM measurements carried out under vacuum conditions (data not shown) revealed a remarkable shrinkage of the fibrils, which was likely because of the loss of water molecules from the fibrillar structures upon extensive drying. This evidence is consistent with the observed dependence of the protein conductivity on the relative humidity, confirming the primary role of water molecules (e.g., hydration shells) in the charge-transport mechanism.

In addition to electrical conductivity, we discovered that poly(ValGlyGlyLeuGly) nanofibrils display an intrinsic blue-green fluorescence upon near-UV/blue excitation. Fig. 5 shows two representative fluorescence images of the fibrillar nanostructures obtained by confocal microscopy (excitation wavelength, 405 nm). These samples were prepared by means of the same cast-deposition procedure used for scanning probe measurements by using two different concentrations of the polypentapeptide (Fig. 5*a*, 1 mg/ml; Fig. 5*b*, 0.1 mg/ml). Spatially resolved fluorescence experiments revealed the typical structural features of the fibrils, which are similar to those observed by AFM. Fig. 5*a* shows a region of high-fibril density (near the edge of the deposited drop), in which the presence of large amorphous aggregates is clearly visible, along with a dense carpet (layer) of close fibrillar structures. Notably, in these regions, the polypeptide aggregates seem to act as fibrillogenesis nuclei, from which most of the fibrillar structures radiate. This finding was observed in different regions of the same sample, as well as in other solid-state samples realized with the same fibril concentration by both confocal and AFM measurements. However, such peculiar features were not found in less concentrated samples (see Fig. 5*b*), suggesting that such large structures arise from extensive (random) aggregation of many fibril molecules occurring at high-protein concentrations. At any rate, more detailed and specific investigations might further clarify the possible role of peptide aggregates in the fibrillogenesis mechanism and/or in the fibrils self-assembling in the solid state.

Single fibrils randomly distributed onto the silicon substrate and characterized by a remarkable degree of morphological heterogeneity are clearly visible in samples prepared from more diluted suspensions (Fig. 5*b*). In line with AFM experiments (see Fig. 1*a*), the presence of some small aggregates also is detectable (Fig. 5*b*). The possibility of imaging such small protein structures reveals the great potential of the direct (label-free) excitation of the self-assembled polypeptides, e.g., to investigate the aggregation state or the polymorphism of amyloid-like fibrils (and possibly of other proteinaceous material) by fluorescence microscopy even in the absence of aromatic residues, such as in the case of the poly(ValGlyGlyLeuGly).

Some single, bright protein filaments also are detectable in Fig. 5*a*, such as the long fibril (arrow). A line profile of this structure is reported in Fig. 6*a*, revealing a diameter of ≈1 μm (in this figure, the presence of many less bright fibrillar structures in the submicrometer range also may be observed). Spectral analysis of the native fluorescence of the self-assembled polypeptides discloses a broadband emission (≈95-nm spectral width) centered at ≈465 nm (Fig. 6*b*). No significant emission shifts were observed by analyzing the fluorescence spectra from large aggregates or single fibrils, although a detailed, high-resolution examination of the line shapes of the emission spectra still needs to be carried out, owing to the noisy spectra from most single fibrils or smaller regions within individual structures (brighter samples by specifically designed experiments might reveal an interesting dependence of the spectral features on the conformational/aggregation state of the biomolecules). Interestingly, preliminary time-resolved experiments performed by collecting the fluorescence signals over wide areas (i.e., without spatial resolution) indicated average lifetimes in the range of a few nanoseconds, with significant variations depending on the ex-

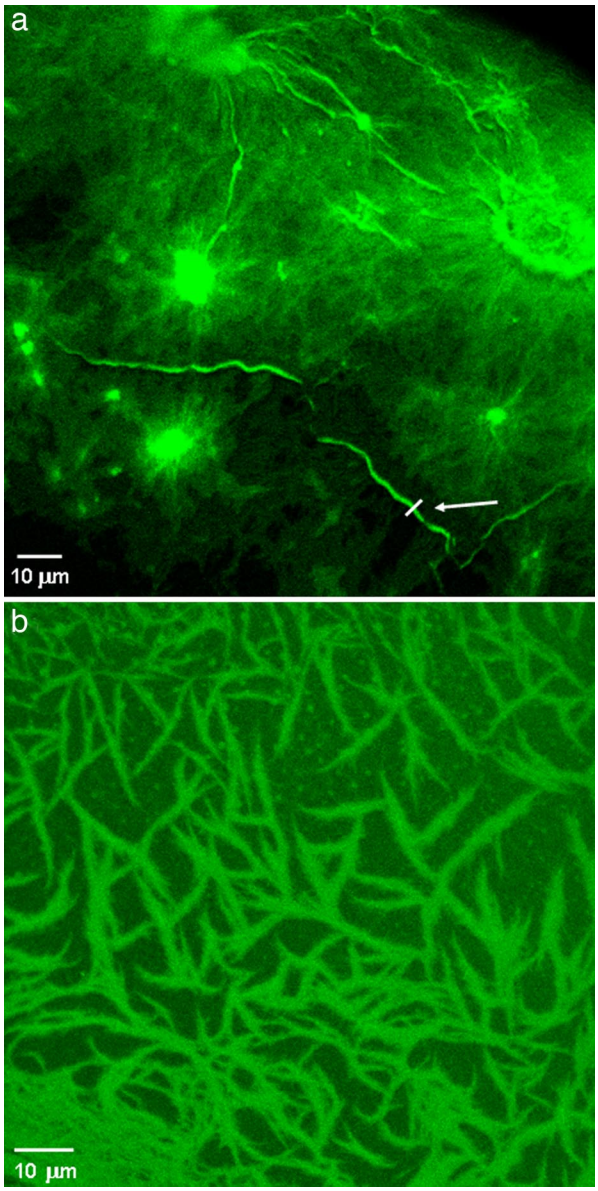

Fig. 5. Confocal microscopy images of the poly(ValGlyGlyLeuGly) amyloid-like fibrils. Fluorescence experiments were performed on the same samples used for AFM characterizations by using two different concentrations of the fibril suspension. (*a*) Concentration at 1.0 mg/ml. (*b*) Concentration at 0.1 mg/ml. The excitation wavelength was 405 nm.

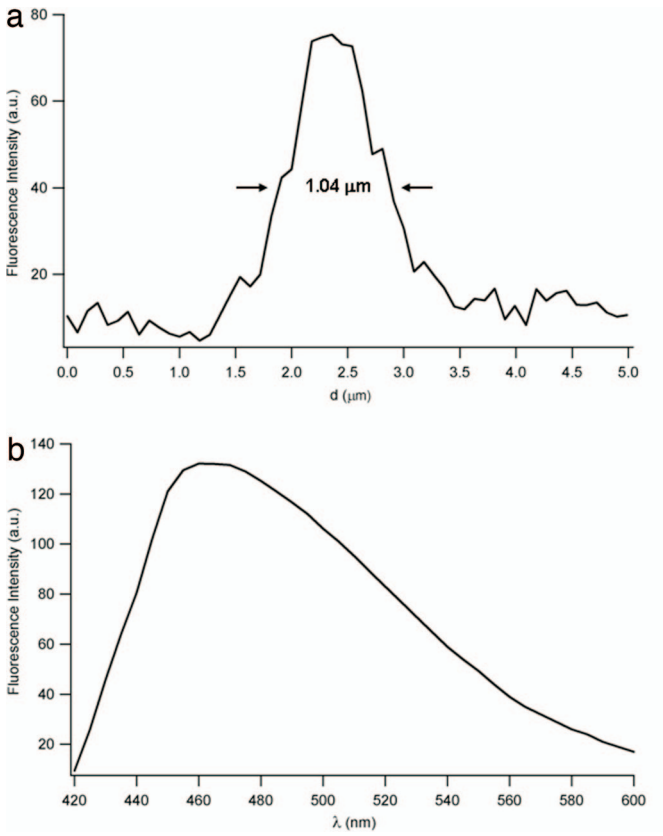

Fig. 6. Fluorescence analysis of the nanofibrils. (*a*) Fluorescence line profile of the single fibril indicated by the arrow in Fig. 5*a*. (*b*) Intrinsic fluorescence spectrum of the self-assembled polypeptides (excitation wavelength, 405 nm; emission bandwidth, 10 nm).

cited region (the excitation spot size was a few millimeters squared). The typical lifetime fits were always multiexponential (usually three or four) and changed markedly according to the inspected region. This finding reflects the high conformational heterogeneity of the sample and suggests a possible correlation between this photophysical parameter and the polypeptides' conformational patterns. If confirmed by spatially resolved, time-resolved experiments (e.g., by fluorescence lifetime imaging microscopy techniques), such an intrinsic feature would offer an extremely attractive method for the investigation of the folding properties of proteins and polypeptides. We also have observed that the intrinsic luminescence of the fibrils can be photobleached, and that the same fluorescence images can be obtained by two-photon excitation, although with low efficiency (data not shown).

The physical mechanism underlying the intrinsic fluorescence emission is unknown, but it may be argued that the charge transport and photoluminescence properties exhibited by unmodified fibrils could be strictly related. It is possible that direct excitation of the fibrils may induce electronic transitions in peptides (e.g., in amide groups) because of a partial delocalization of peptide electrons elicited by the presence of hydrogen bonds (amyloid fibers are characterized by the cross-β structure, in which extensive hydrogen bonding occurs, largely mediated by trapped water molecules) (Fig. 7) (9–12). Such electronic delocalization also may occur in the solid state thanks to the significant retention of water molecules at ambient conditions (such as hydration shells and other water molecules present in the inner structure of the nanofibrils). Peptide excitations can partially relax by fluorescence processes, whereas the electronic delocalization may account for the observed conductivity of the fibrils. This hypothesis is consistent with the experimental evidence of poor conductivity in vacuum conditions. When water molecules are lost by the fibrillar structures, hydrogen bonds collapse and, in turn, electronic delocalization is strongly reduced. Thus, solid-state fibrils might support a network of delocalized electrons that can tunnel through the peptide backbone and hydrogen bond networks, creating charge-transfer pathways between different parts of a polypeptide or fibril molecule. Importantly, fluorescence measurements performed under vacuum conditions strongly support such assumptions about the fluorescence/transport mechanisms (SI Fig. 9). The fluorescence emission, in fact, was found to be strongly dependent on the retention of water molecules; that is, the fluorescence signal underwent a significant decrease in intensity under vacuum conditions (>70% of the fluorescence signal was lost, compared with the same samples maintained at ambient con-

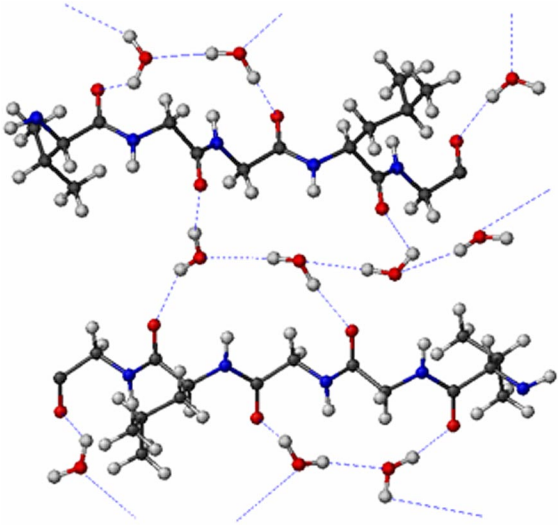

Fig. 7. Model for the extensive interaction of poly(ValGlyGlyLeuGly) with water.

ditions) (SI Fig. 9). When fibril samples were brought back to ambient conditions, the fluorescence signal was completely recovered. This experimental evidence strongly suggests that the water molecules bound to the proteins play a key role in the fluorescence emission of the fibrils. It is important to point out that such behavior is analogous to what we have already observed and discussed for protein conductivity.

We have performed the same characterization experiments (AFM, STM, transport, and fluorescence) on the analogue poly(ValGlyGlyValGly) synthetic polypeptide. Similar results were obtained in terms of morphological, conduction, and luminescence properties, thus confirming the general validity of the presented results. Furthermore, x-ray photoelectron spectroscopy studies on poly(ValGlyGlyValGly) hydrogel (32) demonstrated that the carbonyl groups of the polymers are involved in an extensive set of hydrogen bonds with water. If the same model is applied to poly(ValGlyGlyLeuGly), the previous considerations on charge transport and photoluminescence properties are quite understandable in terms of structure at the atomic level.

In conclusion, we have shown the conductive properties of the fibrillar nanostructures self-assembled from the synthetic poly(ValGlyGlyLeuGly) peptides by STM and two-terminal transport experiments. We observed a remarkable stability of the fibrils at ambient conditions in terms of both morphological and conduction properties, which obviously represents an important aspect from the viewpoint of device implementation. We also demonstrated native fluorescence of the nanofibrils, which allows for direct imaging of their folding and aggregation properties.

The peculiar features of these peptide nanostructures, along with the possibility to specifically modify and manipulate their aminoacidic sequence by genetic engineering techniques, may provide several advantages for their use in future applications in biomolecular electronics and nanobiotechnology. Experiments aimed at controlling the assembly of single-peptide fibrils onto desired locations with precise orientations (by direct interaction with SAM patterns, covalent bonds to specific residues, or microfluidics techniques) and investigating their elastic properties (by AFM spectroscopy) are currently underway in our laboratories.

Materials and Methods

Sample Preparation. The polypentapeptides poly(ValGlyGlyLeuGly) and poly(ValGlyGlyValGly) were chemically synthesized according to the procedures previously developed by Tamburro and colleagues (29, 34).

Fibrils were generated by suspending the dry powder peptide at a concentration of 1.0 mg/ml in Milli-Q water (Millipore Corporation, Billerica, MA) and incubating the solution in a vial tube for 3–5 weeks at 27°C to obtain mature amyloid-like fibrils (29).

AFM Measurements. Fibril samples were prepared by cast deposition of a 20-μl drop of 0.1 mg/ml diluted fibril suspension onto an SiO_2 substrate. After solvent evaporation, the protein structures were characterized by AFM (in tapping mode). All AFM experiments were performed in air at ambient conditions (20–25°C, atmospheric pressure, 50–60% humidity). AFM images were taken by using a CP-II scanning probe microscope (Digital Instruments, Santa Barbara, CA) equipped with 5- or 100-μm scanners (0.5/1 Hz scan rate). Standard silicon probes (MPP-11100; Veeco Probes, Camarillo, CA) with a nominal spring constant of 40 N/m and a resonance frequency of 300 kHz were used.

STM Measurements. STM images were acquired in air at room temperature by using a multimode scanning probe microscope (Digital Instruments) equipped with an E-scanning head (maximum scan size, 10 μm). For these experiments, the 0.1 mg/ml fibril suspension in ultrapure water was deposited onto gold substrates by means of the same procedure used for silicon dioxide. Before fibril deposition, STM analyses (data not shown) confirmed the presence of atomically flat 111 Au terraces of $\approx$0.5-nm height. STM images were taken in constant current mode with a typical tunneling current of 50–150 pA and a bias voltage of 0.1 V (0.5–1 Hz scan rate). The samples were scanned with mechanically prepared platinum/iridium STM tips (PT-ECM; Veeco Probes). During STM imaging, several control experiments were carried out to ensure that the real structures of the fibrils were observed, instead of artifacts from the substrate or tip features.

Transport Measurements. The conductive properties of the fibrils were investigated by two-terminal transport experiments performed onto interdigitated electrodes. The fibrils were deposited onto the electrodes structures by cast deposition of a 10-μl drop of the 0.1 mg/ml fibrils suspension in ultrapure water (Millipore). The sample was then maintained overnight at ambient conditions. Such a procedure resulted in efficient fibrils deposition across the electrodes. The presence of polypentapeptide fibrils between electrodes was carefully assessed by SEM (150 E-beam lithography system; Raith, Ronkonkoma, NY) and AFM analyses.

The devices for our transport experiments consisted of interdigitated electrodes fabricated on thermally oxidized silicon wafers using standard photolithographic techniques. The structure consisted of interdigitated gold lines of 2-μm width and 40-nm height and a line-space period of 2–10 μm, covering an active area of 400 $\times$ 500 μm^2. Control experiments carried out on empty devices (i.e., without fibrils) revealed low-current signals (always $<$1 pA) (Fig. 4 *Inset*). The sample current was measured by means of a probe station (Karl Suss, Waterbury Center, VT) combined with a parameter analyzer (Agilent Technologies, Palo Alto, CA) and a cryogenic system (MMR Technologies, Mountain View, CA).

Confocal Microscopy Experiments. Spatially resolved fluorescence images of the fibrils were taken by a confocal microscope (TCS-SP5; Leica, Wetzlar, Germany). These experiments were performed on the same samples used for AFM characterizations by using two different concentrations of the fibril solution (0.1 and 1.0 mg/ml). The excitation wavelength was 405 nm. Samples were observed through a 63$\times$, 1.40 NA oil-immersion objective.

For spectral analysis, the excitation wavelength was 405 nm, and the emission bandwidth was 10 nm.

We thank F. Calabi for fruitful discussions, M. R. Armenante and G. Lanza (University of Basilicata, Potenza, Italy) for a computer-generated model of hydrated poly(VGGLG), and E. D'Amone and P. Cazzato for technical assistance. This work was supported by the Italian Ministry of Research (Fondo per l'Incentivazione della Ricerca di Base Project RBLA03ER38_001) and the European Union (Elastage Contract 018960).

1. Whitesides GM, Mathias JP, Seto CT (1991) *Science* 254:1312–1319.
2. Dobson CM (1999) *Trends Biochem Sci* 24:329–332.
3. Rochet JC, Lansbury PT, Jr (2000) *Curr Opin Struct Biol* 10:60–68.
4. Pepys MB (2001) *Philos Trans R Soc London B* 356:203–210.
5. Dobson CM (2001) *Biochem Soc Symp* 68:1–26.
6. Guijarro JI, Sunde M, Jones JA, Campbell ID, Dobson CM (1998) *Proc Natl Acad Sci USA* 95:4224–4228.
7. Gross M, Wilkins DK, Pitkeathly MC, Chung EW, Higham C, Clark A, Dobson CM (1999) *Protein Sci* 8:1350–1357.
8. Serpell LC (2000) *Biochim Biophys Acta* 1502:16–30.
9. Jimenez JL, Guijarro JI, Orlova E, Zurdo J, Dobson CM, Sunde M, Saibil HR (1999) *EMBO J* 18:815–821.
10. Perutz MF, Finch JT, Berriman J, Lesk A (2002) *Proc Natl Acad Sci USA* 99:5591–5595.
11. Makin OS, Atkins E, Sikorski P, Johansson J, Serpell LC (2005) *Proc Natl Acad Sci USA* 102:315–320.
12. Kishimoto A, Hasegawa K, Suzuki H, Taguchi H, Namba K, Yoshida M (2004) *Biochem Biophys Res Commun* 315:73–745.
13. Laidman J, Forse GJ, Yeates TO (2006) *Acc Chem Res* 39:576–583.
14. Gazit E (2002) *Angew Chem Int Ed Engl* 41:257–259.
15. Dobson CM (2002) *Nature* 418:729–730.
16. Koga T, Taguchi K, Kobuke Y, Kinoshita T, Higuchi M (2003) *Chemistry* 9:1146–1156.
17. MacPhee CE, Dobson CM (2000) *J Am Chem Soc* 122:12707–12713.
18. Kozel BA, Wachi H, Davis EC, Mecham RP (2003) *J Biol Chem* 278:18491–18498.
19. Tamburro AM, Pepe A, Bochicchio B, Quaglino D, Ronchetti IP (2005) *J Biol Chem* 280:2682–2690.
20. Reches M, Gazit E (2003) *Science* 300:625–627.
21. Scheibel T, Parthasarathy R, Sawicki G, Lin XM, Jaeger H, Lindquist SL (2003) *Proc Natl Acad Sci USA* 100:4527–4532.
22. Jayawarna V, Ali M, Jowitt TA, Miller AF, Saiani A, Gough JE, Ulijn R, (2006) *Adv Mater* 18:611–614.
23. Zhang S (2003) *Nat Biotechnol* 21:1171–1178.
24. Ryadnov MG, Woolfson DN (2003) *Nat Mater* 2:329–332.
25. Kasai S, Ohga Y, Mochizuki M, Nishi N, Kadoya Y, Nomizu M (2004) *Biopolymers* 76:27–33.
26. Mesquida P, Ammann DL, MacPhee CE, McKendry RA (2005) *Adv Mater* 17:893–897.
27. Horii A, Wang X, Gelain F, Zhang S (2007) *PLoS ONE* 2:e190.
28. Reches M, Gazit E (2006) *Nat Nanotech* 1:195–200.
29. Flamia R, Zhdan PA, Martino M, Castle JE, Tamburro AM (2004) *Biomacromolecules* 5:1511–1518.
30. Pompa PP, Bramanti A, Maruccio G, del Mercato LL, Cingolani R, Rinaldi R (2005) *Chem Phys Lett* 404:59–62.
31. Pompa PP, Della Torre A, del Mercato LL, Chiuri R, Bramanti A, Calabi F, Maruccio G, Cingolani R, Rinaldi R (2006) *J Chem Phys* 125: 021103.
32. Flamia R, Salvi AM, D'Alessio L, Castle JE, Tamburro AM (2007) *Biomacromolecules* 8:128–138.
33. Wang Z, Zhou C, Wang C, Wan L, Fang X, Bai C (2003) *Ultramicroscopy* 97:73–79.
34. Tamburro AM, Guantieri V, Gordini DD (1992) *J Biomol Struct Dyn* 10:441–454.